# Coherent Optical RF Channelizer With Large Instantaneous Bandwidth and Large In-Band Interference Suppression

Zhenzhou Tang, *Student Member, IEEE*, Dan Zhu, *Member, IEEE, Member, OSA*, and Shilong Pan, *Senior Member, IEEE, Senior Member, OSA*

***Abstract*—RF channelization is regarded as one of the most effective approaches to relieve the difficulty of processing wideband signals in microwave and millimeter-wave receivers. In this paper, a novel coherent optical RF channelizer with broad instantaneous bandwidth and large in-band interference suppression is proposed and demonstrated based on a multichannel photonic image-reject mixer (IRM). A Ku-band RF signal with an instantaneous bandwidth of 5 GHz is sliced into five consecutive subchannels with 1-GHz instantaneous bandwidth by the proposed channelizer. The in-band interference suppression, which relies on the image-rejection ratios of the IRM, is about 25 dB. To the best of our knowledge, the proposed channelizer achieves the highest in-band interference suppression in such wide instantaneous bandwidth.**

***Index Terms*—Channelizer, frequency mixing, image reject, microwave photonics, optical frequency comb.**

## I. Introduction

WITH the increasing of signal bandwidth in modern RF systems such as radars, electronic warfare, navigation, and wireless communications and satellite communications, receivers with the capability of processing wideband RF signals are urgently needed. Channelization is one of the most effective methods that can fulfill this requirement by slicing the received broadband RF signal into a number of narrowband channels. Owing to the benefits in terms of broad bandwidth, low loss, and immunity to electromagnetic interference, photonics-based RF channelization has attracted a great deal of attention over the last two decades. Several schemes have been reported to perform the RF channelization in the optical domain, which can be generally classified into three categories:

Manuscript received November 24, 2017; revised March 19, 2018; accepted July 13, 2018. Date of publication July 19, 2018; date of current version August 30, 2018. This work was supported in part by the National Natural Science Foundation of China under Grant 61422108 and Grant 61527820, in part by the Natural Science Foundation of Jiangsu Province under GrantBK20160082, in part by Jiangsu Provincial Program for High-level Talents in Six Areas (DZXX-030), in part by the Funding for Outstanding Doctoral Dissertation in NUAA under Grant BCXJ16-04, and in part by the Fundamental Research Funds for the Central Universities. *(Corresponding author: Shilong Pan.)*

The authors are with the Key Laboratory of Radar Imaging and Microwave Photonics, Ministry of Education, Nanjing University of Aeronautics and Astronautics, Nanjing 210016, China (e-mail: tangzhzh@nuaa.edu.cn; danzhu@nuaa.edu.cn; pans@ieee.org).

Color versions of one or more of the figures in this paper are available online at http://ieeexplore.ieee.org.

Digital Object Identifier 10.1109/JLT.2018.2857500

In the first category, a series of optical filters with consecutive passbands are applied to slice the modulated optical RF signal into a number of sub-channels. The optical filter array can be realized by phase-shifted fiber Bragg gratings (FBGs) [1], Bragg-grating Fabry-Perot cavities [2], or acousto-optic filters [3]. To ensure adequate processing bandwidth and sufficient suppression of spurs and crosstalk, a large number of optical filters with flat-top and steep-edge frequency responses are usually required, which significantly increases the difficulties of device fabrication, and makes wavelength alignment of these optical filters extremely challenging.

In the second category, the RF spectrum is first copied to a series of optical carries from an optical frequency comb (OFC) generator, and then a comb filter with a free spectral range (FSR) that is slightly different from that of the OFC is employed to select different slices of the RF spectrum from different optical copies. Since these RF components are well separated in the wavelength domain, a wavelength-division multiplexer is sufficient to split them into a series of sub-channels. Previously, a Fabry-Perot filter [4], two Fabry-Perot filters with different FSRs [5], and multiple stages of optical ring lattices [6], [7] were employed to serve as the optical comb filter.

One critical problem associated with the approaches in the above two categories is that after channelization the detailed information in the RF signal will be lost and unrecoverable due to the spectrum aliasing caused by the square-law detection of photodetectors (PDs). To overcome this problem, coherent optical RF channelizer was proposed, in which multiple different local oscillators (LOs) are used to downconvert different spectral slices of the RF signal to a common baseband or intermediate frequency (IF) band. The multiple LOs can be produced by a pair of OFCs with slightly different FSRs [8]–[11]. When the received RF signal is broadcasted to one of the OFCs, different part of the RF signal would be downconverted due to the frequency beating with the nearest comb line from the other OFC. The spectrum aliasing problem caused by the square-law detection of PDs can be solved by in-phase/quadrature (I/Q) demodulation based on balanced photodetection and electrical digital signal processing (DSP) [8], [10]. Restricted by the bandwidth and effective-number-of-bit of analog-to-digital converters (ADCs) in the DSP, the instantaneous bandwidth of the OFC-based coherent optical RF channelizer is only hundreds of MHz [8]. Furthermore, due to the uneven and asymmetrical phase and amplitude responses of the in-phase (I) and quadrature (Q) branches in the I/Q demodulator, large suppression of the in-band interference or crosstalk in a broad bandwidth is extremely difficult. As a result, only single-tone or quite narrow-band (several kHz or MHz) RF signals were channelized in the previous-reported RF channelizers [8]–[10]. Recently, we have reported a coherent RF channelizer based on dual OFCs and a multichannel image-reject mixer (IRM), which can achieve broad instantaneous bandwidth and large in-band interference suppression [12], but only some preliminary experimental results were reported.

In this paper, a more comprehensive study on the coherent RF channelizer based on the dual OFCs and the multichannel IRM is performed. A detailed theoretical analysis is carried out. Since the spectrum aliasing problem solved in the analog domain by the multichannel photonic IRM, no electrical ADCs are required in the channelizer, so the instantaneous bandwidth of each channel is significantly increased. In addition, the IRM implemented in the optical domain can achieve large image-reject ratio in a broad bandwidth, which leads to RF channelization with large in-band interference suppression. An experiment is carried out. A 5-GHz RF signal covering nearly the entire Ku-band (13–18 GHz) is channelized into five consecutive sub-channels. The in-band interference suppression ratio is around 25 dB within the 1-GHz instantaneous processing bandwidth. The spurious free dynamic range (SFDR) of the proposed channelizer is about 93 dB$\cdot$Hz$^{2/3}$.

## II. Principle

Fig. 1(a) shows the schematic diagram of the proposed coherent optical RF channelizer based on the multichannel photonic IRM, which mainly consists of modules for signal OFC generation, local OFC generation, and multichannel image-reject mixing.

### A. Signal OFC Generation

In the proposed system, a continuous-wave (CW) light generated by a laser diode (LD) is split into two branches by a 50:50 optical coupler. In the upper branch, the optical carrier is sent to a Mach-Zehnder modulator (MZM) which is driven by a single-tone microwave signal with a frequency of $f_{\mathrm{S}}$. If the power of the drive signal is high enough, an OFC, denoted as signal OFC thereafter, can be generated,

$$\begin{aligned} f_{\mathrm{sig-OFC}}\left(t\right) &= E_{\mathrm{in}}\left[1+\cos\left(\frac{\pi}{V_\pi}V_{\mathrm{S}}\cos(2\pi f_{\mathrm{S}}t)+\frac{\pi}{V_\pi}V_{\mathrm{bias}}\right)\right] \\ &= \sum_{m=1} A_m \exp\left\{j2\pi\left[f_{\mathrm{sig}}+(m-1)f_{\mathrm{S}}\right]t\right\} \end{aligned} \tag{1}$$

where $E_{\mathrm{in}}$ is the electrical field of the optical carrier, $V_{\mathrm{S}}$ is the amplitude of the input driving signal, $V_\pi$ is the half-wave voltage of the MZM, $V_{\mathrm{bias}}$ is the DC bias voltages applied to the MZM. $f_{\mathrm{sig}}$ is the frequency of the first comb line, and $A_m$ is the amplitude of the $m^{th}$-order comb line. The signal OFC is then modulated by a received wideband RF signal via a dual-drive Mach-Zehnder modulator (DMZM). By using optical single sideband (OSSB) modulation based on a 90-degree electrical hybrid ($\mathrm{EH}_1$) [13], the generated sidebands would only locate at the right (or left) side of each comb line of the signal OFC. If the received wideband RF signal is denoted as $f_{\mathrm{RF}}(t)$, the signal OFC with RF modulation can be written as

$$\begin{aligned} f_{\mathrm{sig-mod}}\left(t\right) = &\sum_{m=1} A_m \exp\left\{j2\pi\left[f_{\mathrm{sig}}+(m-1)f_{\mathrm{S}}\right]t\right\} \\ &+\gamma\sum_{m=1} A_m \exp\left\{j2\pi\left[f_{\mathrm{sig}}+(m-1)f_{\mathrm{S}}\right]t \right. \\ &\left. + f_{\mathrm{RF}}\left(t\right)\right\} \end{aligned} \tag{2}$$

where $\gamma$ is a parameter related to the modulation index. The optical spectrum at the output of the DMZM is shown in Fig. 1(b). The modulated signal is amplified by an erbium-doped fiber amplifier ($\mathrm{EDFA}_1$) and sent to the signal port of a 90-degree optical hybrid.

### B. Local OFC Generation

In the lower branch, the optical carrier is first sent to an optical frequency shifter, in which the optical carrier is modulated by a sinusoidal signal with a frequency of $f_{\mathrm{D}}$ via a phase modulator, and the $+1^{\mathrm{st}}$-order sideband is selected by an optical bandpass filter (OBPF). After being amplified by a second EDFA ($\mathrm{EDFA}_2$), the up-shifted optical carrier is applied to a polarization modulator (PolM), which is driven by an LO with a frequency of $f_{\mathrm{L}}$. According to [14], by properly setting both the power of the LO and the polarization state, a flat OFC (denoted as local OFC thereafter) can be produced, which is given by

$$f_{\mathrm{local-OFC}}\left(t\right) = \sum_{m=1} B_m \exp\left\{j2\pi\left[f_{\mathrm{LO}}+(m-1)f_{\mathrm{L}}\right]t\right\} \tag{3}$$

where $f_{\mathrm{LO}}$ is the frequency of the first comb line of the local OFC, and $B_m$ is the amplitude of the $m^{\mathrm{th}}$-order comb line. The optical spectrum of the local OFC is shown in Fig. 1(c). If the frequencies of the $n^{\mathrm{th}}$-order comb lines of the signal OFC and local OFC equal to the optical carriers, the relationship of $f_{\mathrm{LO}}$ and $f_{\mathrm{D}}$ can be expressed as

$$\begin{aligned} f_{\mathrm{D}} &= \left[f_{\mathrm{LO}}+(n-1)f_{\mathrm{L}}\right]-\left[f_{\mathrm{sig}}+(n-1)f_{\mathrm{S}}\right] \\ &= \left(f_{\mathrm{LO}}-f_{\mathrm{sig}}\right)+(n-1)\left(f_{\mathrm{L}}-f_{\mathrm{S}}\right) \end{aligned} \tag{4}$$

Furthermore, as can be seen from (3), for the $m^{\mathrm{th}}$-order comb lines from the signal OFC and the local OFC, they have a frequency difference of

$$f_\Delta^{(m)} = \left[f_{\mathrm{LO}}-f_{\mathrm{sig}}\right]+(m-1)\left(f_{\mathrm{L}}-f_{\mathrm{S}}\right) \quad m=1,2,\ldots \tag{5}$$

From (5), the frequency difference is consisted of a constant component (the first term at the right side), which equals to the frequency difference between $f_{\mathrm{LO}}$ and $f_{\mathrm{sig}}$, and a variable component (the second term at the right side), which is determined by both the order of the comb lines and the frequency difference between $f_{\mathrm{L}}$ and $f_{\mathrm{S}}$. Thus, an equivalent multiple LOs at the frequency of $f_\Delta^{(m)}$ are generated. The generated local OFC is

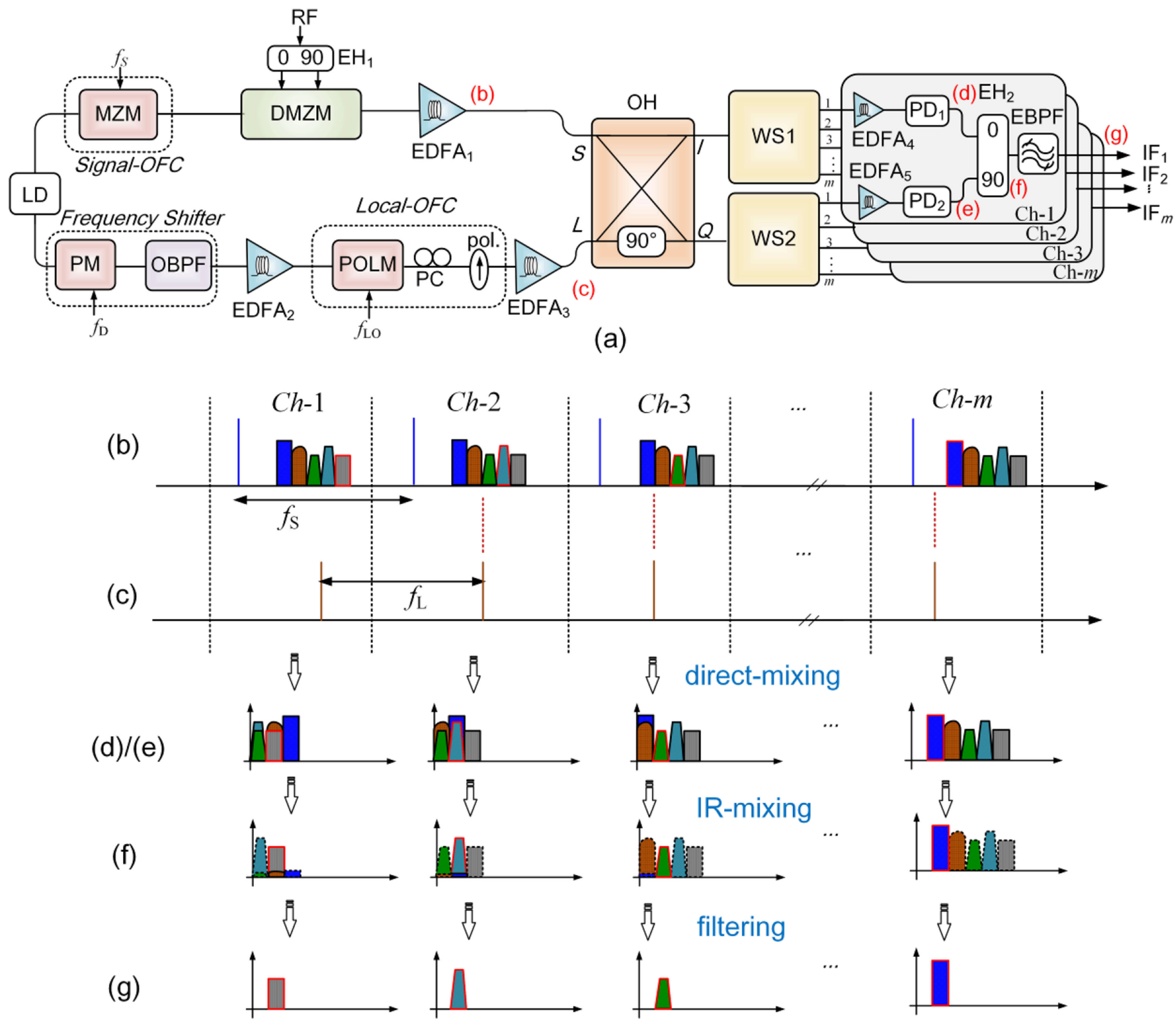


Fig. 1. (a) Schematic diagram of the proposed coherent optical RF channelizer. (b)–(g) Illustrations of the optical and electrical spectra at different points of the channelizer. LD: laser diode; MZM: Mach-Zehnder modulator; PM: phase modulator; DMZM: dual-drive MZM; PolM: polarization modulator; PC: polarization controller; Pol.: Polarizer; EDFA: erbium-doped fiber amplifier; OH: optical hybrid; EH: electrical hybrid; PD: photodetector; OBPF: optical bandpass filter; EBPF: electrical bandpass filter.

amplified by $\mathrm{EDFA}_3$ and sent to the LO port of the 90-degree optical hybrid.

### *C. Multichannel Image-Reject Mixing*

The I and Q outputs of the 90-degree optical hybrid are sent to a pair of parallel filters, respectively. The primary function of the parallel filters is to split the I and Q output signals into several independent channels. In each channel, as can be seen from the dashed lines in Fig. 1(b) and (c), the I and Q outputs consist of a modulated RF sideband from the signal OFC and an unmodulated comb line from the local OFC, which can be written as

$$\begin{aligned} I(t) &= \gamma A_m \exp\{j2\pi[f_{\mathrm{sig}} + (m-1)f_{\mathrm{S}}]t + f_{\mathrm{RF}}(t)\} \\ &\quad + B_m \exp\{j2\pi[f_{\mathrm{LO}} + (m-1)f_{\mathrm{L}}]t\} \\ Q(t) &= \gamma A_m \exp\{j2\pi[f_{\mathrm{sig}} + (m-1)f_{\mathrm{S}}]t + f_{\mathrm{RF}}(t)\} \\ &\quad + jB_m \exp\{j2\pi[f_{\mathrm{LO}} + (m-1)f_{\mathrm{L}}]t\} \end{aligned} \tag{6}$$

When the two signals are amplified and applied to two PDs ($\mathrm{PD}_1$ and $\mathrm{PD}_2$), a pair of quadrature frequency-downconverted outputs can be obtained

$$\begin{aligned} i_{\mathrm{I}}(t) &\propto A_m B_m \cos\left\{2\pi\left[f_{\mathrm{RF}}(t) - f_{\Delta}^{(m)}\right]\right\}t \\ i_{\mathrm{Q}}(t) &\propto A_m B_m \sin\left\{2\pi\left[f_{\mathrm{RF}}(t) - f_{\Delta}^{(m)}\right]\right\}t \end{aligned} \tag{7}$$

Since $f_{\Delta}^{(m)}$ is different in each channel, different parts of the received RF signal would be downconverted in each channel (as depicted in Fig. 1(d)/(e)). However, the frequency components at the left and right sides of the LO comb line will be simultaneously downconverted to the baseband, which causes a strong in-band interference that cannot be removed by electrical filtering.

To solve this problem, a photonics-based multichannel IRM is employed. Fig. 2 shows the general principle diagram of the IRMs [15]. When an RF signal is mixed with a pair of quadrature LOs, two quadrature outputs are obtained. If the

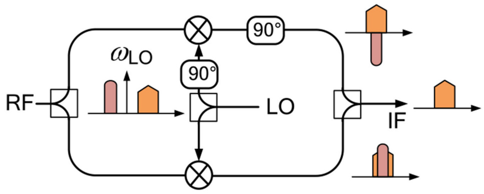


Fig. 2. General principle diagram of image-reject mixers.

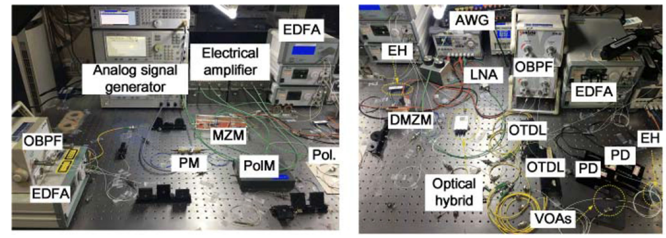


Fig. 3. Photograph of the experimental setup.

two signals are combined by a 90-degree electrical hybrid, the signal downconverted from the right (or left) side of the LO would be enhanced while that downconverted from the other side will be eliminated. Therefore, the output of the IRM would be only contributed by the component at one side of the LO. In the proposed scheme, since a pair of quadrature downconverted signals have already been obtained at the outputs of $PD_1$ and $PD_2$, image-reject mixing can be easily achieved when a second electrical hybrid ($EH_2$) is connected to combine them [16]. By this way, only the components at the right side of the local comb line will be downconverted to the baseband, and the signals downconverted from the other side will be greatly suppressed, as shown in Fig. 1(f). Finally, an electrical bandpass filter (EBPF) is connected to remove the out-of-band signals (Fig. 1(g)).

As the comb lines of the local OFC align to different locations of the modulated RF sideband in different channels, different spectral slices of the RF signal would be downconverted to the same IF band. In addition, the spectral components of interests are actually separated by a spacing of $f_L$, which could be tens of GHz, so a multichannel programmable filter with a low resolution or a wavelength-division demultiplexer is sufficient to split them into sub-channels. Moreover, unlike the I/Q demodulation based on DSP used in [8], [10], the problem of information aliasing is solved by the multichannel photonics-based IRM in the analog domain, which can support much broad instantaneous processing bandwidth and high processing speed. Furthermore, since the optical hybrid has a relatively low phase and amplitude imbalances, high image-reject ratio can be obtained [16], by which the in-band interference can be significantly suppressed within a large frequency range. It should be noted that the conversion efficiency in each channel is slightly different, due to the difference of the amplitudes of the comb lines, as can be seen from (7). This problem can be solved by tuning the optical power in each channel or applying an optical line-by-line spectrum reshaper to make the combs flat. Another notable thing is that, since the signal OFC and local OFC share a common LD, the phases of the signal OFC and local OFC can be ignored in the analysis, and no optical carrier phase extraction and tracking is needed.

## III. Experiment and Results

### A. System Structure

An experiment based on the configuration shown in Fig. 1(a) is carried out. Fig. 3 shows the picture of the experimental setup. A CW optical carrier with a wavelength of 1550.55 nm and a power of 19 dBm is generated by an LD (TeraXion PS-NLL-1550) and split into two equal parts by an optical coupler. In the upper branch, the optical carrier is sent to a 40-Gb/s MZM (Fujitsu FTM7938) with a half-wave voltage of 3.5 V. The MZM is driven by a 25-GHz single-tone signal, which is generated by an analog signal generator (Agilent E8257D). An electrical power amplifier (Agilent 83020A, 2–26.5 GHz) is used to boost the RF power. The generated signal OFC is then sent to a DMZM (Fujitsu FTM7937) with a half-wave voltage of 3.5 V. A wideband RF signal from an arbitrary waveform generator (Keysight M9502A) is amplified by an electrical low noise amplifier and spilt into two quadrature parts by a 90-degree electrical hybrid ($EH_1$, Krytar 3017360 K, 1.7–36 GHz). The quadrature outputs of $EH_1$ are applied to the two RF ports of the DMZM. By properly setting the bias voltage applied to the DMZM, OSSB modulation is realized. The output signal of the DMZM is amplified by an EDFA and sent to the signal port of a dual-polarization 90-degree optical hybrid (Kylia COH28). In the lower branch, the optical carrier is sent to a phase modulator (EOSpace AZ-AV5-40) which is driven by a 14-GHz single-tone signal produced by an analog signal generator (Agilent N5183B). An OBPF (Yenista XTM-50) is inserted to select the $+1^{st}$-order sideband to achieve optical frequency up-shifting. After being amplified by $EDFA_2$, the optical sideband goes through a PolM (Versawave Technologies Inc.) driven by a 24-GHz single-tone signal, a polarization controller, and a polarizer to generate a local OFC. The generated local OFC is amplified by $EDFA_3$ and send to the LO port of the optical hybrid. The I and Q outputs of the optical hybrid from the same channel are sent to $PD_1$ and $PD_2$ with bandwidths of 10 GHz and responsivities of 0.8 A/W, after being amplified by $EDFA_4$ and $EDFA_5$, respectively. Then, the outputs of $PD_1$ and $PD_2$ are combined by a low-frequency (1–2 GHz) 90-degree electrical hybrid ($EH_2$), to achieve image-reject mixing. An optical tunable delay line (OTDL, General Photonics) and a variable optical attenuator (VOA) are inserted in each branch to compensate the phase and amplitude imbalances. Finally, an EBPF with a passband of 1–2 GHz is connected to remove the out-of-band frequency components. The optical spectrum is measured by an optical spectrum analyzer (YOKOGAWA AQ6370C), and the electrical spectrum is observed by a 40-GHz electrical spectrum analyzer (R&S FSV-40).

Due to the limitation of the facilities in our lab, two tunable optical bandpass filters (Yenista XTM-50) are inserted in the I and Q branches of the optical hybrid to perform channel selection. Thus, the channelization is tested channel by channel by tuning the center wavelengths of the optical filters. Since the parallel filters can be achieved by commercially-available

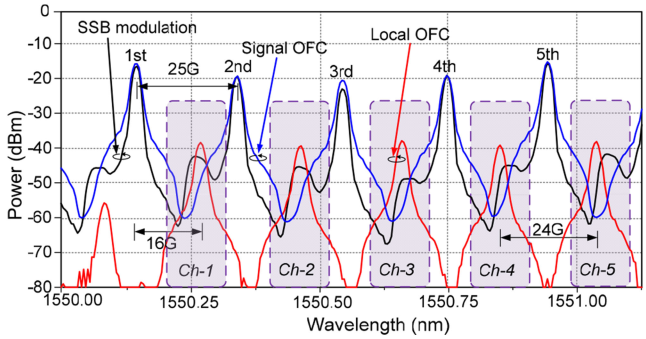


Fig. 4. Optical spectra of the local OFC (red line), signal OFC (blue line) and signal OFC with RF modulation (black line).

TABLE I
PARAMETERS OF THE EXPERIMENT SETUP

| Symbo l | Parameter | Value |
|---|---|---|
| $f_S$ | FSR of signal OFC | 25 GHz |
| $f_L$ | FSR of local OFC | 24 GHz |
| $f_D$ | Frequency shift | 14 GHz |
| $f_{sig}$ | Frequency of the 1st line of signal OFC | / |
| $f_{LO}$ | Frequency of the 1st line of local OFC | / |
| $f_{LO}$–$f_{sig}$ | Frequency difference of the 1st comb lines between the local OFC and signal OFC | 16 GHz |
| $m$ | Channel number | 1~5 |
| $f_\Delta^{(m)}$ | Equivalent LO in $m^{th}$ channel | (17-$m$) GHz |

waveshapers (e.g., Finisar 16000S) or wavelength-division demultiplexers (if $f_S$ and $f_L$ are large enough to match the spacing of the demultiplexer), the demonstration in this experiment can be easily extended to parallelized multichannel. In addition, since only the outputs from one polarization of the optical hybrid are used in the experiment, the polarization states of the local OFC and signal OFC should be identical to achieve the highest conversion efficiency. However, if more PDs are available, the outputs from the orthogonal branch of the optical hybrid can also be taken part in the channelization, so the performance of the channelizer would be insensitive to the polarization states of the input signals [17].

## B. Dual OFCs Generation

Fig. 4 shows the measured optical spectra of the local OFC, signal OFC and signal OFC with RF modulation. The blue line represents the signal OFC obtained at the output of the MZM. As can be seen, a 5-line OFC with an FSR of 25 GHz is generated. The frequencies of each comb line of the signal OFC are $f_{\rm sig}$, $f_{\rm sig}+25$, $f_{\rm sig}+50$, $f_{\rm sig}+75$, $f_{\rm sig}+100\,$GHz, and the frequency of the middle comb line equals to the optical carrier frequency. Then the signal OFC is modulated by a wideband LFM signal. Due to the OSSB modulation, a sideband is produced at the right side of each comb line of the signal OFC, as can be seen from Fig. 4 (the black line). The red line in Fig. 4 shows the optical spectrum of the local OFC, which also has five comb lines but has an FSR of 24 GHz. The frequencies of the comb lines of the local OFC are $f_{\rm LO}$, $f_{\rm LO}+24$, $f_{\rm LO}+48$, $f_{\rm LO}+72$, $f_{\rm LO}+96\,$GHz, in which the middle comb line denotes the optical carrier. As the optical carrier that used to generate the local OFC is up-shifted by 14 GHz as compared with the carrier of the signal OFC, thus $(f_{\rm LO}+48)$- $(f_{\rm sig}+50)=14\,$GHz. In other words, the frequency difference between the first comb lines of the local OFC and signal OFC is 16 GHz, i.e., $f_{\rm LO}-f_{\rm sig}=16\,$GHz. Besides, since $f_{\rm L}-f_{\rm S}=-1\,$GHz, the equivalent LO, according to (4), is $(17-m)$ GHz in each channel. Table I summarizes the descriptions and values of the key parameters of the experiment setup.

## C. Multichannel Image-Reject Mixing

In the first step, we investigate the performance of the image-reject mixing in each channel. Since the instantaneous sub-channel bandwidth of the designed channelizer is set to be 1 GHz, in this demonstration, a linear frequency-modulated (LFM) signal with 1-GHz bandwidth is employed as the received RF signal.

According to the parameters in Table I, the equivalent LO $(f_\Delta^{(1)})$ is 16 GHz in *Ch-1*. Locations of the RF, LO, and image are shown as the inset in Fig. 5(a). The black solid line in Fig. 5(a) depicts the electrical spectrum of the downconverted IF signal when a 17–18 GHz LFM is applied to the DMZM. An IF signal with a center frequency of 1.5 GHz and a power spectral density (PSD) of about $-109.8$ dBm/Hz is obtained. The red dashed line in Fig. 5(a) shows the electrical spectrum when the center frequency of the LFM signal is changed to be 14.5 GHz (i.e., image frequency). The PSD of the downconverted IF signal is dropped to around $-134.8$ dBm/Hz, so the image-reject ratio in *Ch-1* is 25 dB within a bandwidth of 1 GHz. Fig. 5(b)–(e) show the results obtained in other four channels. As can be seen, image-reject mixings are realized in each channel, and the measured image-reject ratios are all around 25 dB, which means that only the frequency components at the right side of the local comb line with a frequency difference of 1–2 GHz will be downconverted in each channel. The spectra of the input RF signals are also presented as the blue solid lines in Fig. 5. As can be seen, the conversion loss is about 25 dB.

## D. RF Channelization

Then, a wideband LFM signal covering 13–18 GHz with a PSD of $-89.8$ dBm/Hz is applied to the proposed channelizer. The inset in Fig. 6(a) illustrates the locations of the modulated sideband and the corresponding local comb line in *Ch-1*. Due to the frequency beating between the modulated sideband and the local comb line, a downconverted signal located at 0–3 GHz is produced at the output of $\rm PD_1$ (and $\rm PD_2$), which is shown as the dashed line in Fig. 6(a). Since the components downconverted from 16–18 GHz and 13–16 GHz would be spectrally superimposed, which cannot be separated and analyzed independently, an instantaneous frequency-time (IFT) analysis method based on short-time Fourier transform (STFT) is employed to verify the image rejection [18]. By using the IFT analysis method, the frequency-time relationship would be extracted, so that the signals can be distinguished as long as their frequency-time

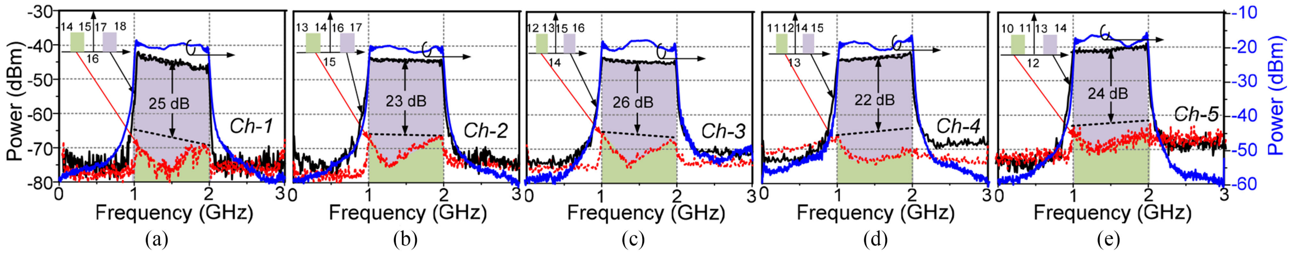


Fig. 5. (a)–(e) Electrical spectra of the IF signals downconverted from the RF signal (black solid line) and the downconverted image (red dashed line) in *Ch-1* to *Ch-5* (resolution bandwidth: 3 MHz). Blue line: the electrical spectra of the input RF signal. Inset: the location illustration of the image, LO and RF signals in each channel.

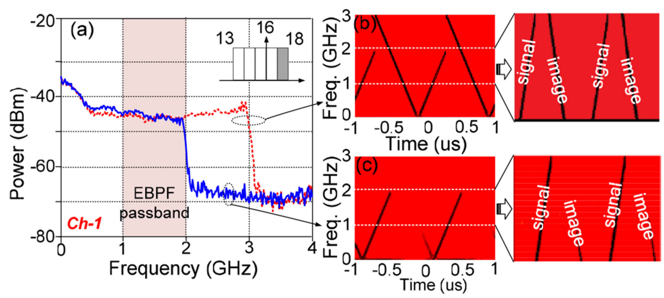


Fig. 6. (a) Electrical spectra of the IF signals at the output of $PD_1$ (red dashed line) and $EH_2$ (black solid line) in *Ch-1,* and (b), (c) the corresponding instantaneous frequency-time diagrams.

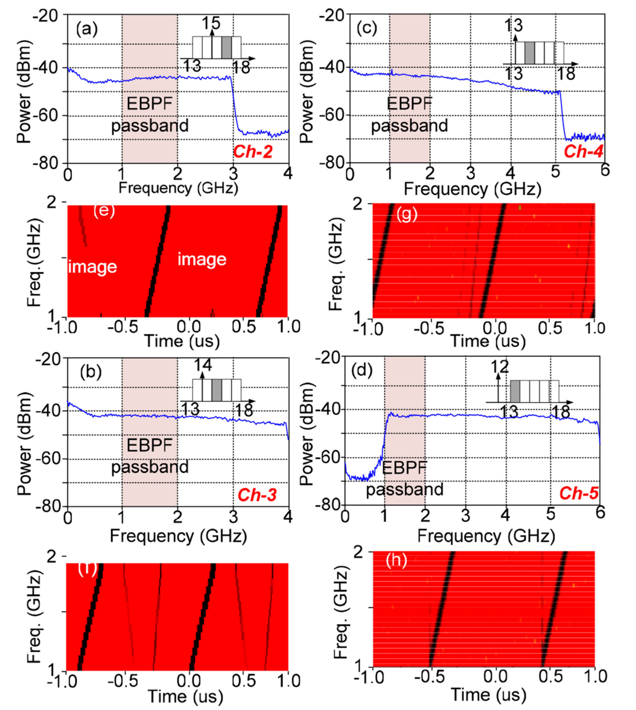


Fig. 7. (a)–(d) Electrical spectra of the signals at the output of *Ch-2* to *Ch-5,* and (e)–(h) the corresponding instantaneous frequency-time diagrams in 1–2 GHz.

relationships are different, even though they are located in the same frequency range. As can be seen from the IFT diagram in Fig. 6(b), both the up- and down-chirped signals exist in the channel passband (i.e., 1–2 GHz). The solid line in Fig. 6(a) shows the electrical spectrum when the outputs of $PD_1$ and $PD_2$ are combined by $EH_2$. Since the signal downconverted from 13–16 GHz is suppressed by the IRM, only a 0–2 GHz signal is obtained. Besides, from the IFT diagram in Fig. 6(c), a strong up-chirped signal and a quite weak down-chirped signal (image) are existed in the channel passband, showing that the in-band interference is largely suppressed. With the 1–2 GHz components selected by the EBPF, the downconverted spectral slice of the input RF signal located at 17–18 GHz (gray-shaded box in the inset) is finally achieved.

Similar results are obtained in other channels, as shown in Fig. 7:

i) In *Ch-2*, the input RF signal is mixed with a 15 GHz LO to produce a 0–3 GHz signal (Fig. 7(a)), and from the IFT diagram in Fig. 7(e), the final output of *Ch-2* is downconverted from the spectral slice of the input RF signal located at 16–17 GHz;

ii) In *Ch-3*, the input RF signal is mixed with a 14 GHz LO to produce a 0–4 GHz signal (Fig. 7(b)), and from the IFT diagram in Fig. 7(f), the final output of *Ch-3* is downconverted from the spectral slice of the input RF signal located at 15–16 GHz;

iii) In *Ch-4*, the input RF signal is mixed with a 13 GHz LO to produce a 0–5 GHz signal (Fig. 7(c)), and from the IFT diagram in Fig. 7(g), the final output of *Ch-4* is downconverted from the spectral slice of the input RF signal located at 14–15 GHz;

iv) In *Ch-5*, the input RF signal is mixed with a 12 GHz LO to produce a 1–6 GHz signal (Fig. 7(d)), and from the IFT diagram in Fig. 7(h), the final output of *Ch-5* is downconverted from the spectral slice of the input RF signal located at 13–14 GHz.

Therefore, based on the proposed channelizer, the received 5-GHz-bandwidth RF signal can be channelized into five consecutive channels with 1-GHz bandwidth. The in-band interference can be suppressed by about 25 dB thanks to the multichannel photonic microwave IRM.

The SFDR of the proposed channelizer is also measured. Taking *Ch-1* as an example, a two-tone RF signal (17.49 GHz and 17.51 GHz) is generated and applied to the channelizer. Fig. 8v shows the measured SFDR, which is about 93 dB$\cdot$Hz$^{2/3}$.

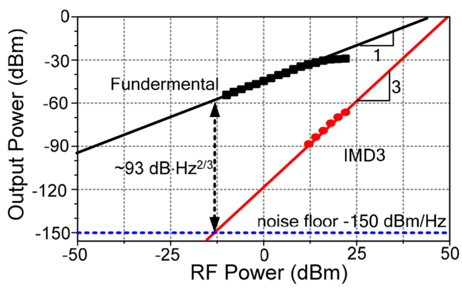


Fig. 8. SFDR measurement of a sub-channel in the proposed channelizer.

Similar results, within 92∼95 dB·Hz$^{2/3}$, are obtained in other sub-channels.

## IV. Discussion

### A. Bandwidth

The instantaneous bandwidth of each channel is determined by both the frequency difference between the FSRs of the signal OFC and the local OFC and the IF bandwidth of the IRM, which is given by

$$\mathrm{BW_{Inst.}} = \min\left\{(f_S - f_L), \mathrm{BW_{IRM}}\right\} \quad (8)$$

where $\mathrm{BW_{IRM}}$ denotes the IF bandwidth of the IRM. Since $f_S - f_L$ can be easily adjusted, the instantaneous bandwidth of the channelizer, in most cases, mainly relies on $\mathrm{BW_{IRM}}$. Thanks to the broadband nature of the photonic components, $\mathrm{BW_{IRM}}$ is mainly restricted by the bandwidth of $EH_2$ and EBPF. Although in the experiment, we set the instantaneous bandwidth as 1 GHz, the actual value can be increased by applying wideband electrical hybrids and EBPFs.

The RF bandwidth of the channelizer is used to characterize the frequency range of the input RF signal, which is determined by the RF bandwidth of the IRM. Because OSSB modulation is employed in the channelizer, the RF frequency should be $< f_S$ to avoid the interference between the neighboring channel, so that the RF bandwidth of the IRM, as well as the channelizer, should be lower than $f_S$. Besides, since the sub-channel bandwidth is $|f_L - f_S|$, the RF bandwidth of the channelizer equals to $m|f_L - f_S|$, if $m$ comb lines take part in the RF channelization. Therefore, the RF bandwidth of the channelizer is given by

$$\mathrm{BW_{RF}} = \min\left\{f_S, m\left|f_L - f_S\right|\right\} \quad (9)$$

In the proposed channelizer, the demonstrated RF bandwidth is 13–18 GHz, which can be further extended by increasing the comb-line number and the FSRs of the OFCs, as can be seen from (9).

### B. Interference Suppression

There are two main kinds of interference that should be taken into consideration, which are in-band interference and out-of-band interference. The out-of-band interference can be easily removed by EBPFs since they usually fall out of the passband of the channel. The in-band interference has two primary sources. On the one hand, the non-ideal OSSB modulation may have a residual $-1^{\mathrm{st}}$-order sideband. If a wideband RF signal is applied to the channelizer, the desired $+1^{\mathrm{st}}$-order sideband in one channel will be partly superimposed with the undesired $-1^{\mathrm{st}}$-order sideband in the adjacent channel. Although this kind of interference cannot be removed through filtering or image-reject mixing, it can be eliminated if the FSRs of the OFCs are larger than twice of the signal bandwidth. On the other hand, the frequency components presented at the other side of the local comb line could have a frequency offset to the comb line that is equal to the IF frequency, which introduces the dominant in-band interference. Although it would be very large, it can be efficiently suppressed by the photonics-based multichannel IRM. In the experiment, the in-band interference suppression ratio is around 25 dB in all channels. Table II compares the in-band interference suppression performance between the proposed channelizer and other electrical and optical ones. As can be seen, although some methods can achieve higher image rejection ratio [10], [20], the suppression ratio is optimized only for a single-tone signal [10], or the instantaneous bandwidth is quite narrow [20]. Therefore, the instantaneous bandwidth (1 GHz) with 25-dB image-suppression ratio is much larger than the commercially available electrical devices and the previously reported photonics-based IRMs.

TABLE II
In-Band Interference Suppression Comparison

| Ref. | E/O | RF BW [GHz] | IBW [GHz] | Supp. Ratio [dB] |
|---|---|---|---|---|
| *This work* | O | 13-18 | 1 | ~25 (wideband) |
| [8] | O | 3.75-7.25 | 0.5 | NA |
| [9] | O | NA | 0.08 | NA |
| [10] | O | 15.5-37.1 | 1.2 | 60 (single tone) |
| [11] | O | 0-20 | 1 | NA |
| [19] | E | 6-18 | <0.21 | 23 |
| [20] | E | 1.75-8.75 | 0.4375 | 11~32 |

Inst. BW: instantaneous bandwidth; Supp. Ratio: suppression ratio; single tone: the suppression ratio is optimized only for a single-tone signal.

## V. Conclusion

A coherent optical RF channelizer with broad instantaneous bandwidth based on a multichannel photonic IRM has been proposed. With the multiple LOs generated by the dual OFCs, different spectral parts of the received RF signal is downconverted to a common IF band. More importantly, making use of the multichannel photonic IRM, the in-band interference is largely suppressed. An experiment is carried out. A Ku-band RF signal covering 13–18 GHz is sliced into five sub-channels based on the proposed channelizer. The in-band interference suppression ratio is ∼25 dB for all sub-channels. The measured SFDR is about 93 dB·Hz$^{2/3}$. The proposed channelizer can find applications in photonics-based radar and electrical warfare systems.

## References


[1] D. B. Hunter and R. A. Minasian, "Microwave optical filters using in-fiber Bragg grating arrays," *IEEE Microw. Guided Wave Lett.*, vol. 6, no. 2, pp. 103–105, Feb. 1996.

[2] S. T. Winnall, A. C. Lindsay, M. W. Austin, J. Canning, and A. Mitchell, "A microwave channelizer and spectroscope based on an integrated optical bragg-grating Fabry–Perot and integrated hybrid fresnel lens system," *IEEE Trans. Microw. Techn.*, vol. 54, no. 2, pp. 868–872, Feb. 2006.

[3] P. F. Snawerdt III, D. Koontz, R. K. Morse, and N. C. Hollingsworth, “Acousto-optic channelizer-based ultra-wideband signal processor,” U.S. Patent 6 091 522, Jul. 18, 2000.
[4] X. Xie *et al.*, “Broadband photonic radio-frequency channelization based on a 39-GHz optical frequency comb,” *IEEE Photon. Technol. Lett.*, vol. 24, no. 8, pp. 661–663, Apr. 2012.
[5] X. Zou, W. Pan, B. Luo, and L. Yan, “Photonic approach for multiple-frequency-component measurement using spectrally sliced incoherent source,” *Opt. Lett.*, vol. 35, no. 3, pp. 438–440, Feb. 2010.
[6] X. Gu, D. Zhu, S. Li, Y. Zhao, and S. Pan, “Photonic RF channelization based on series-coupled asymmetric double-ring resonator filter,” in *Proc. 7th IEEE Int. Conf. Adv. Infocomm Technol.*, 2014, pp. 240–244.
[7] J. R. Adleman, S. Zlatanovic, J. M. Kvavle, B. M. L. Pascoguin, and E. W. Jacobs, “High finesse compound optical ring filter for parametric multicasting RF channelization,” in *Proc. IEEE Int. Top. Meeting Microw. Photon.*, 2013, pp. 257–260.
[8] X. Xie *et al.*, “Broadband photonic RF channelization based on coherent optical frequency combs and I/Q demodulators,” *IEEE Photon. J.*, vol. 4, no. 4, pp. 1196–1202, Aug. 2012.
[9] W. Y. Xu, D. Zhu, and S. L. Pan, “Coherent photonic RF channelization based on dual coherent optical frequency combs and stimulated brillouin scattering,” *Opt. Eng.*, vol. 55, no. 4, Apr. 2016, Art. no. 046106.
[10] A. O. J. Wiberg *et al.*, “Coherent filterless wideband microwave/ millimeter-wave channelizer based on broadband parametric mixers,” *J. Lightw. Technol.*, vol. 32, no. 2, pp. 3609–3617, Oct. 2014.
[11] W. Hao *et al.*, “Coherent wideband microwave channelizer based on dual optical frequency combs,” in *Proc. IEEE Avionics Veh. Fiber-Opt. Photon. Conf.*, 2016, pp. 183–184.
[12] Z. Z. Tang, D. Zhu, and S. L. Pan, “Coherent RF channelizer based on dual optical frequency combs and image-reject mixers,” in *Proc. Int. Top. Meeting Microw. Photon.*, 2017, pp. 1–4.
[13] G. H. Smith, D. Novak, and Z. Ahmed, “Overcoming chromatic-dispersion effects in fiber-wireless systems incorporating external modulators,” *IEEE Trans. Microw. Techn.*, vol. 45, no. 8, pp. 1410–1415, Aug. 1997.
[14] C. He, S. L. Pan, R. H. Guo, Y. J. Zhao, and M. H. Pan, “An ultra-flat optical frequency comb generated based on cascaded polarization modulators,” *Opt. Lett.*, vol. 37, no. 18, pp. 3834–3836, Sep. 2012.
[15] R. Hartley, “Single-sideband modulator,” U.S. Patent 1 666 206, Apr. 1928.
[16] Z. Z. Tang and S. L. Pan, “A reconfigurable photonic microwave mixer using a 90-degree optical hybrid,” *IEEE Trans. Microw. Techn.*, vol. 64, no. 9, pp. 3017–3025, Sep. 2016.
[17] D.-S. Ly-Gagnon, S. Tsukamoto, K. Katoh, and K. Kikuchi, “Coherent detection of optical quadrature phase-shift keying signals with carrier phase estimation,” *J. Lightw. Technol.*, vol. 24, no. 1, pp. 12–21, Jan. 2006.
[18] H. K. Kwok and D. L. Jones, “Improved instantaneous frequency estimation using an adaptive short-time Fourier transform,” *IEEE Trans. Signal Process.*, vol. 48, no. 10, pp. 2964–2972, Oct. 2000.
[19] Krytar Inc, “3-dB 90 degree hybrid couplers.” [Online]. Available: http://krytar.com/products/hybrid-couplers/3-db-90-degree-hybrid-couplers/
[20] V. Singh, T. Forbes, W. G. Ho, J. Ko, and R. Gharpurey, “A 16-band channelizer employing harmonic rejection mixers with enhanced image rejection,” in *Proc. IEEE Custom Integr. Circuits Conf.*, 2014, pp. 1–4.

**Zhenzhou Tang** (S’14) received the M.S. degree in information engineering from Nanjing University of Aeronautics and Astronautics, Nanjing, China, in 2014. He is currently working toward the Ph.D. degree at the Key Laboratory of Radar Imaging and Microwave Photonics, Ministry of Education, Nanjing University of Aeronautics and Astronautics.

He is also a visiting Ph.D. student with the Photonics Research Group, Ghent University, Ghent, Belgium. His research interests include photonic generation of microwave signals, photonic integrated circuits, and photonics-based microwave mixing. He has authored or coauthored more than 30 research papers, including more than 15 papers in peer-reviewed journals and 15 papers in conference proceedings. He is also one of the recipients of 2017 IEEE Photonics Society Graduate Student Fellowship.

**Dan Zhu** (M’12) received the B.S. and Ph.D. degrees in electronics engineering from Tsinghua University, Beijing, China, in 2004 and 2009, respectively.

In 2009, she joined the Research Department of Radar Signal Processing, the 14th Research Institute, China Electronics Technology Group Corporation, as a Researcher. In 2011, she joined the Key Laboratory of Radar Imaging and Microwave Photonics, Ministry of Education, Nanjing University of Aeronautics and Astronautics, Nanjing, China, where she is currently an Associate Professor. Her current research interests include photonic microwave and millimeter wave generation and optical signal processing.

Dr. Zhu is a member of the IEEE Microwave Theory and Techniques Society, the IEEE Photonics Society, and the Optical Society of America.

**Shilong Pan** (S’06–M’09–SM’13) received the B.S. and Ph.D. degrees in electronics engineering from Tsinghua University, Beijing, China, in 2004 and 2008, respectively. From 2008 to 2010, he was a “Vision 2010” Postdoctoral Research Fellow with the Microwave Photonics Research Laboratory, University of Ottawa, Ottawa, ON, Canada. In 2010, he joined the College of Electronic and Information Engineering, Nanjing University of Aeronautics and Astronautics, Nanjing, China, where he is currently a Full Professor. He is the Deputy Director with the Key Laboratory of Radar Imaging and Microwave Photonics, Ministry of Education, Nanjing University of Aeronautics and Astronautics. His research has focused on microwave photonics, which includes optical generation and processing of microwave signals, analog photonic links, photonic microwave measurement, and integrated microwave photonics. He has authored or coauthored more than 380 research papers, including more than 200 papers in peer-reviewed journals and 180 papers in conference proceedings.

Prof. Pan is currently a Topical Editor of *Chinese Optics Letters*, and he is a Technical Committee member of IEEE MTT-3 Microwave Photonics. He is a Steering Committee Member of IEEE International Topical Meeting on Microwave Photonics and International Conference on Optical Communications and Networks. He has also served as a Chair of a number of international conferences, symposia, and workshops, including the TPC Chair of the International Conference on Optical Communications and Networks in 2015, TPC Co-Chair of IEEE International Topical Meeting on Microwave Photonics in 2017, TPC Subcommittee Chair or Co-Chair of the IEEE Radio Wireless Symposium in 2013, 2014, and 2016, the OptoElectronics and Communication Conference in 2015, CLEO Pacific Rim in 2018, the International Conference on Information Optics and Photonics in 2018, and the Chair of the microwave photonics for broadband measurement workshop of International Microwave Symposium in 2015. He is a Fellow of the IET and a senior member of the OSA. He was selected to receive an OSA outstanding reviewer award in 2015 and a top reviewer of IEEE/OSA JOURNAL OF LIGHTWAVE TECHNOLOGY in 2016. He was the recipient of the Excellent Young Scholars Award of the National Natural Science Foundation of China in 2014, and the Scientific and Technological Innovation Leading Talents Award of the National Ten Thousand Plan in 2018.